NORTHERN ILLINOIS UNIVERSITY

Autophagy in DNA-PKcs Knockout Glioblastoma Cancer Stem Cells

A Capstone Submitted to the

University Honors Program

In Partial Fulfillment of the

Requirements of the Baccalaureate Degree

With Honors

Department of

Biological Sciences

By

Samantha Diulus

DeKalb, Illinois

11 May 2019

University Honors Program
Capstone Approval Page

Capstone Title: Autophagy in DNA-PKcs Knockout Glioblastoma Cancer Stem Cells

Student Name (print or type): Samantha Diulus

Faculty Supervisor (print or type): Dr. Linda Yasui

Faculty Approval Signature: Linda Yasui

Department of (print or type): Biological Sciences

Date of Approval (print or type): 2/7/2019

Check if any of the following apply, and please tell us where and how it was published:

☐ Capstone has been published (Journal/Outlet):

_____

☐ Capstone has been submitted for publication (Journal/Outlet):

_____

☐ Capstone has been presented (Conference):

_____

☐ Capstone has been submitted for presentation (Conference):

_____

Completed Honors Capstone projects may be used for student reference purposes, both electronically and in the Honors Capstone Library (CLB 110).
If you would like to opt out and not have this student's completed capstone used for reference purposes, please initial here: _____ (Faculty Supervisor)

Abstract

Glioblastoma multiforme (GBM) is a deadly form of brain cancer, with an expected survival of only a few months after diagnosis without therapy. The current standard of care extends life expectancy by a couple of months due to almost universal recurrence of the tumor. Recurrence of GBM is highly dependent on a radiation-resistant subpopulation of GBM, the cancer stem cells (CSCs). CSCs possess an enhanced ability to repair therapy-induced DNA damage, especially DNA double strand breaks (DSBs). To study the role of DNA damage repair in GBM CSCs, our investigations used a knockout (KO) of an enzyme, DNA PKcs, which plays a key role in the repair of DNA double strand breaks. Surprisingly, we discovered that autophagy (assayed by the direct visualization of autophagosomes) wasprofoundly affected by DNA PKcs KO in GBM cells and GBM CSCs. Furthermore, exposure of these cells to 2Gy irradiation caused another shift in autophagy. Changes in mitochondrial morphology raised questions regarding energy metabolism, prompting the use of an ATP assay that indicated increased energy requirements in cells lacking DNA-PKcs. These results point to a role for cancer cell energy metabolism and cancer stem cell metabolism in the cells' therapeutic response, emphasizing the importance of understanding the stress responses of GBM cells and GBM cancer stem cells to improve radiation treatment against cancer.

Introduction

Glioblastoma multiforme (GBM) is a lethal form of brain cancer. The current standard of care, which includes temozolomide combined with radiation therapy post-operatively, only increases survival from 12 to 15 months (Stupp et al. 2009). In an attempt to develop novel therapeutic approaches, some researchers have targeted tumor cell metabolism. Haines and Miklos (2014) adding an angiogenesis inhibitor, bevacizumab, to the typical therapeutic regime. Unfortunately, early results from clinical trials indicate that bevacizumab does not improve overall survival in newly diagnosed GBM. Despite these aforementioned efforts and those made by other researchers (Marie et al. 2011; Poteet et al. 2013), the notion of targeting cancer cell metabolism continues to be pursued. These previous studies have only explored treatment of differentiated tumor cell types, however, the tendency of the cancer stem cell (CSC) type to resist current treatments makes it a promising target for new therapeutic strategies.

CSCs are a population of cells with stem cell-like qualities that allow them to differentiate into the wide variety of tumorigenic cell types. This property contributes to the phenotypic and functional heterogeneity that is typical of tumors, resulting in resistance to treatment, treatment failure, and ultimately recurrence (Francesco et al. 2018). Therefore, understanding and targeting CSCs may improve the effectiveness of treatment modalities. Metabolism is considered a relevant feature of CSCs, contributing to and maintaining stemness. In order to better understand this resistant "cancer stem cell state" and the unique metabolism that is associated with it, it is important that the level of autophagy and ATP metabolism in irradiated and unirradiated GBM cells is surveyed.

Since CSCs have an enhanced ability to repair radiation-induced DNA damage, aspects of these repair pathways are important targets for investigation. DNA-PKcs is a gene that is activated upon recognition of DNA damage, initiating the DNA damage response (DDR). In normal cells, DNA-PK phosphorylates AMPK in order to initiate one of two pathways. The first pathway involves the activation of mTOR, which inhibits autophagy (Davis et al. 2014). The second pathway activates Atg, which induces autophagy (Davis et al. 2014). It is important to note that radiation therapy is cytotoxic because of its ability to create double stranded breaks (DSBs). Therefore, the DNA-PK knockout is of great importance and interest because it can cause cells to be genetically predisposed to treatment sensitivity by interrupting the DDR.

In addition to activation of DNA damage repair pathways, DNA damage can induce stress responses in cells, including autophagy. It has been proposed that autophagy and other metabolic checkpoints are responsible for the conversion of metabolic disturbances into vital or lethal stimuli (Green et. al, 2014). This argument suggests that multiple signals dispatched to the cell death-regulatory system converge to induce autophagy. Through this process, cells are able to adapt by utilizing products of degradation, eliminate damaged materials, and traffick recycled cellular contents to revitalize cells with the metabolic building blocks required to overcome or survive stress (Yang & Klinosky 2010). Alternatively, this process can result in lethal stimuli via too much or too little autophagy (Levine 2007). One of the three pillars of cancer treatment, radiation, induces autophagy at the cellular level in virtually every tumor model system (Sharma et al. 2014).

Studies have shown that autophagy induction alone or in combination with other therapeutic strategies results in cell death and acts as a radiation sensitizer (Zois & Koukourakis 2009). Therefore, it is possible that the sensitivity to treatment caused by the DNA-PK knockout combined with induction of autophagy above basal levels can improve therapeutic outcomes in GBM patients.

Alterations in metabolic processes within CSCs extend beyond autophagy induction. In human breast cancer stem cells, an increased number of mitochondria are associated with greater DNA repair potential (Francesco et. al, 2018). This increased mitochondrial content is believed to be a product dynamic mitochondrial movement and asymmetrical apportioning of mitochondria within stem cells. These processes are unusual and may contribute to the stem features in CSCs, aiding in their identification (Francesco et. al, 2018). Quantifying the level of ATP metabolism within CSCs can lend information regarding the number of mitochondria and their collective efficiency. Ultimately, understanding any and all of these processes can open doors to increased survival time for GBM patients.

Methods

Cell Culture. Exponentially growing cultures of U87 (p53-proficient) GBM cells were maintained in monolayer culture in DMEM:F12 (1:1) medium (GIBCO Life Technologies, Grand Island, NY) containing 10% fetal bovine serum (GIBCO Life Technologies, Grand Island, NY) and penicillin/streptomycin. These cultures were housed in 37°C and CO_2 gassed incubator. Trypsinization yielded single cell suspensions, which were used to determine cell number via hemocytometer counting as previously described by Yasui & Owens (2012).

Sphere formation. To grow spheres, cells (100,000 cells/mL) were seeded into 24-well plates in neural stem cell medium (NSCM). NSCM consists of DMEM:F12 containing recombinant human epidermal growth factor (20 ng/mL), basic fibroblast growth factor (20 ng/mL), and B27 supplement. The medium was changed every 2 days. By day 3-5, the U87 cells had formed spheres. These glioma spheres are a mixed culture, containing stem-like cells (high capacity for self-renewal), progenitor cells, and differentiated cells.

RNA isolation and qPCR. 0.5-1 x 10^6 cells were harvested and suspended in 1 mL of Trisure (or Trizol) and transferred to a 1.7 mL Eppendorf tubes before being placed in a -70°C freezer. Once the samples were frozen, they were thawed and then kept on ice. 200µL of chloroform was added, the tube was vortexed, and then the samples were placed back on ice for 5 minutes before centrifuging for 15 minutes at 17,000 xg at 4°C. The aqueous layer was then removed and transferred to a new 1.7 mL Eppendorf tube and the remaining phenol/chloroform solution was discarded. 500 µL of isopropanol was added to each sample before inverting the tubes several times to mix the contents. The 5 minutes of icing followed by 15 minutes of centrifuging was repeated prior to decanting the isopropanol and adding 1 mL of 75% EtOH. The tubes were centrifuged again for 5 minutes at 17,000 xg at 4°C then the EtOH was decanted. The pellet was then allowed to dry for 1-2 hours before being re-suspended in 20-30 µL of NF H_2O .

To quantify RNA, the samples were placed at 65°C for 15 minutes to re-suspend the RNA pellet and 1 µL of NF H_2O was loaded into Nanodrop apparatus and labeled as the blank. Then, 1 µL of each RNA sample at a time was loaded into the apparatus and "measure" was selected. Using these results, dilutions were prepared with 2500 ng of RNA in 0.2 mL Eppendorf tubes. 1 µL of Decamers was added to each sample, then the samples were placed in the thermocycler at 70°C for 5 minutes to anneal the primers. Next, Master Mix for cDNA synthesis was prepared for all samples plus one extra. The solution contained 4 µL MLV RT 5x Buffer, 1 µL NF H_2O, 1 µL MLV Reverse Transcriptase, and 1 µL 10mM dNTPs per reaction. 7 µL of the aforementioned solution was added to each sample before placing them in the thermocycler for 1 hour at 37°C, 5 minutes at 95°C, then finally hold at 4°C. Each sample was diluted with 40 µL NF H_2O.

cDNA samples, molecular marker (CD133, Musashi, SOX2, and Nestin) primers, GADPH primers, and the qPCR plate were kept on ice while the Master Mix was prepared. Samples were run in triplicates for the experimental genes as well as the housekeeping gene. qPCR was run at 95°C for twenty seconds to induce initial denaturation, then cycled 40 times at 95°C for three seconds to further denature, followed by thirty seconds at 60°C to anneal and extend. After 40 cycles were completed, the plate was held at 4°C. Analysis of relative molecular marker mRNA expression was calculated using the $2^{-\Delta\Delta CT}$ method described by Livak and Schmittgen (Livak and Schmittgen, 2001).

Tumorigenesis. Xenotransplantation studies utilized athymic, 5 week old, immunocompromised, female Balb/c nude mice to ensure that the mouse immune system did not interact with the growing tumor. Additionally, the hairless variety was chosen because this feature permits easy visualization of tumors. To prepare the injections, bulk U87 cells were collected by trypsinization before they were resuspended in PBS. To collect CSC, spheres were dissociated with accutase prior to preparing the injection. Following anesthesia with isofluorene gassing, bulk or dissociated CSC were injected into the right or left flank, respectively. At the end of the 6-week study, presence or lack of tumor formation was noted and tumors were excised. The tumors were then embedded in paraffin for sectioning, staining, and histochemistry. All animal protocols were approved by NIU's Office of Research Compliance, Integrity & Safety (ORC #: LA17-0004).

Paraffin embedding and H & E staining. To fix tissues, samples were submerged in 5-10 times their volume of fixative (10% buffered neutral formalin) containing 100 mL 37%-40% formaldehyde, 900 mL distilled water, 4.0 g monobasic sodium phosphate, and 6.5 g dibasic (anhydrous) sodium phosphate. Next, the tissue wasb dehydrated. The tissue was first be placed in 70% alcohol for one hour before being moved to 80% alcohol for two hours. This process was repeated with 90% (2 hours), 95%, (2 hours) and 100% alcohol (overnight). The tissue was then moved to fresh 100% alcohol for one hour before repeating this step once more. Next, the samples were moved to xylene for one hour followed by another hour in fresh xylene. The tissue was then placed in paraffin for two hours (repeat once with fresh

paraffin) and then it was allowed to solidify in the paraffin overnight. Under vacuum, the tissue and paraffin was melted down for 2 hours prior to embedding. To embed tissue samples, paraffin chips were placed in a warmer and, once melted, a drop of paraffin was added to the mold matching the size of the tissue sample. The tissue was then placed into the mold and pressed into the paraffin before filling the rest of the mold with paraffin. After 30 minutes, the paraffin was removed from the mold.

The specimen was then sectioned using a microtome before staining with Harris' Hematoxylin and Eosin. 20 g of aluminum potassium sulfate "alum" was dissolved into 200 mL distilled water while heating, allowing it to almost reach boiling temperature. After returning to room temperature, 1 g hematoxylin was added to 10 mL 100% EtOH and the mixture was shaken before returning it to the heat and bringing it back to boiling temperature for 1 minute or less. The solution was once again removed from the heat before adding 0.5 g mercuric oxide, red (213357). The solution was returned to the heat until it turned dark purple. Then, it was dipped in cold water to cool. Before using the stain, 4 mL glacial acetic acid and filter was added. Slides were heated to 50-60°C prior to deparaffinization and hydration with distilled water. Next, samples were stained in Harris' hematoxylin for 6 to 15 minutes and then washed in tap water for 2 to 5 minutes. Sections were then placed in weak ammonia water or lithium carbonate solution (1.54 g lithium carbonate in 100 mL distilled water) until they turned bright blue (approximately 30 seconds). Again, the slides were washed with tap water for 10 minutes. To complete the staining process, slides samples were placed in 80% EtOH for 1 to 2

minutes, counter-stained with eosin-phloxine solution (25 mL Eosin stock solution, 2.5 mL phloxine stock solution, 195 mL 95% ethyl alcohol, and 1 mL glacial acetic acid) for 2 minutes, and then dehydrated. Finally, specimens were mounted in resinous medium to be imaged. These methods were adapted from those described by Prophet et. al (1992).

Transmission electron microscopy (TEM). Prior to imaging, the cells underwent a multi-day fixation process. To begin, the bulks cells were collected via trypsinization and the CSCs were simply pipetted into a centrifuge tube. The primary fixation utilized Ito and Karnovsky's fixative. 5.0 mL of 1.5% glutaraldehyde in 0.1 M NaCacodylic acid was prepared using 2.5 mL 0.2 M NaCacodylic acid, 2.4 mL water, and 0.1 mL 70% glutaraldehyde. The cells sat in this solution for 1 hour at room temperature. Next, 0.15M NaCocadylic acid was prepared with 2.25 mL 0.2 M NaCacodylic acid and 0.75 mL water. This NaCacodylic acid was used to rinse the cells five times for five minutes each time. The secondary fixative consisted of 2.5 mL 0.2 M NaCacodylic acid, 1 mL osmium tetroxide, and 0.5 mL water to yield 1% osmium tetroxide in 0.125 M NaCacodylate. Again, the cells were placed in this solution for 1 hour at room temperature. After an hour had passed, the cells were rinsed with ddH_2O three times for 8 minutes each time. Following fixation, the cells were treated with 1% tannic acid for 1 hour before being rinsed with ddH_2O three times for 8 minutes each time. The cells were then dehydrated using anhydrous acetone. First, the cells were placed in 70% acetone (0.7 mL acetone: 0.3 mL H_2O) three times for 10 minutes each. Then, the same procedure was followed using 90%

acetone (0.9 mL acetone: 0.1 mL H_2O) and again with 95% acetone (0.95 mL acetone: 0.05 mL H_2O). Finally, the cells were treated with 100% acetone four times for 10 minutes each. Following dehydration, the cells were embedded in Spurrs Epoxy Resin, specifically the A-firm formulation of PolyScience's new "VCD"—standard medium. This resin is composed of 4.1 gm ERL 4221, 1.43 gm Diglydicyl ether of polypropylene glycol (DER 736), 5.9 gm nonenyl succinicic anhydride (NSA), and 0.1 gm dimethylaminoethanol (DMAE). To begin the embedding procedure, the cells were treated with a 1:3 Spurrs:acetone (0.8 mL Spurrs + 2.4 mL acetone) for 45 minutes. Then, for 90 minutes, the cells were placed in a 1:1 Spurrs:acetone mixture (1.5 mL Spurrs + 1.5 mL acetone) before being placed in 3:1 Spurrs:acetone (2.4 mL Spurrs + 0.8 mL acetone) for 4 hours. Finally, the cells were placed in 100% Spurrs Epoxy Resin overnight. To prepare the cells for sectioning and staining, they were pelleted in 100% Spurrs before being decanted and pipetted into BEEM capsules. The BEEM capsules were placed into a 70°C oven to polymerize for 8 hours. The "bullet" was then cut from the capsule.

After fixation and embedding, the bullets were sectioned with the help of a Reichert OM U2 Ultramicrotome before being attached to a TEM grid. Next, the grids were placed in 2% uranyl acetate, section side down, for 5 minutes. Then, the grids were washed three times in 50 mL deionized water and dried with filter paper. For the second phase of the staining procedure, the grids were placed in 0.1% lead citrate for 5 minutes before undergoing three washes. Similar to the first phase of staining, each wash was in 50 mL deionized water, however, the last wash also contained 0.1 mL 10 N NaOH. Again, the grids were dried with filter paper before

imaging. To image the cells, a Hitachi H-600 TEM was used with an acceleration voltage of 75.0 kV.

To analyze and score TEM images for autophagosomes, a few factors determined the presence or absence of these structures. These criteria include size (300-400 nm or 600 nm in cultured cells), presence of a double-membrane, and consistent cytoplasm morphology when compared to the rest of the cell (or partially degraded contents in mature autophagosomes). Additionally, autophagosomes should lack ribosomes on the outer membrane but contain organelles or parts of organelles within their lumen. To effectively score autophagosomes, thirty images of each cell population were collected.

ATP assay. Prior to performing the ATP assay, the CellTiter-Glo reagent (stored at -20°C) was thawed to room temperature in hands. The thawed buffer was then added to the substrate in its amber bottle before vortexing the mixture until the substrate went into solution (less than 1 minute). The ATP solution that is used for this assay was1 mM in concentration and was prepared using 55 mg disodium salt ATP and 10 mL water.

For each population of cells, 6 plates were prepared as a serial dilution of ATP. To begin, 0.9 mL DMEM:F12 medium was added to all of the 35mm petri plates. In the first plate, 0.1 mL of the 1 mM ATP solution was added. Then, 0.1 mL of the solution from plate 1 was pipetted to plate 2 to dilute 10 fold. This process was repeated four times, using 0.1 mL of the previous plate's solution each time.

Consequently, the ATP concentrations in this serial dilution ranged from 0.05 mM to 5×10^{-7} mM, increasing 10 fold each plate.

In each of the aforementioned plates, 10^4 to 10^5 U87 cells were seeded 4-5 hours prior to the assay. Additionally, 1 mL of medium was added to another 35mm petri plate to produce a blank plate. Since the assay is temperature sensitive, the plates must be removed from the incubator 30 minutes prior to the assay to permit the cells and medium to reach room temperature. Following this rest period, 1.0 mL of the CellTiter-Glo Reagent was added to each of the 6 plates and then the plates were swirled on an Orbital mixer for 2 minutes.

To measure Relative Light Units (RLUs), the GloMax® 20/20 Luminometer with Single Auto-Injector E5321 wass connected to the computer (using a serial port or serial to USB adapter) and the GloMax® Luminometer software was started. The "Start" button was pressed in the pop-up window, launching Microsoft Excel, and causing the COM Port and Excel lights in the previous window to turn green. The plate's lid was removed prior to placing it in the luminometer and it was covered once it was in the reader to ensure that none of the solution splashed onto the lid. The "Measurement" button was pressed on the luminometer touch screen to take a reading of the RLUs. The value was sent directly to an Excel spreadsheet and recorded as "SAMPLE-00X" followed by the RLU value. This process was repeated for the entire serial dilution as well as the blank plate. Additionally, the procedure was repeated in its entirety for each cell population including U87 WT, U87 WT CSC, U87 KO, U87 CSC KO, U87 KO 2Gy, U87 KO CSC 2Gy, U87 WT CSC 2Gy.

Results

Before exploring the properties of CSCs, it had to be determined that CSCs existed within the cell population. The formation of spheres was the first indicator of the CSC phenotype (Figure 1). After bulk tumor cells were seeded in NSCM on day 1, cells began to grow closer to one another, showing a clear loss of contact inhibition by day 3.

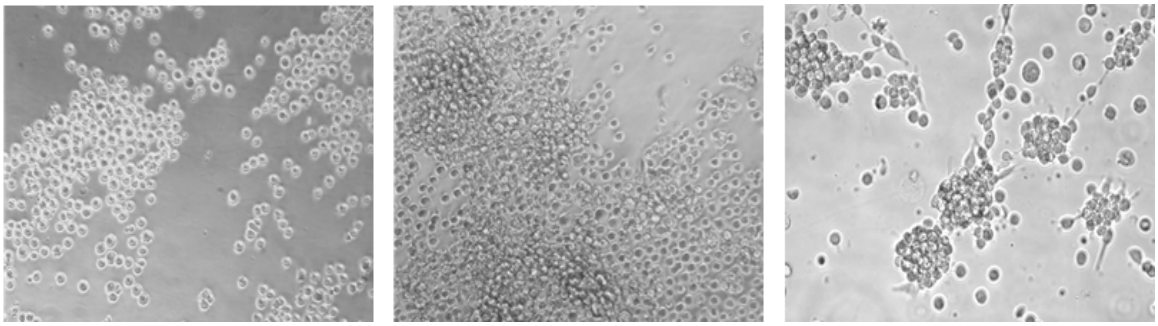

Figure 1. U87 cells form glioma stem cell spheres. U87 cells were plated into NSCM on day 1 (a) and permitted to form U87 tumor initiating spheres or cancer stem cell spheres for 2 (b) or 3 (c) days in NSCM.

In addition to sphere formation, the presence of certain molecular markers is another indicator of the stem cell phenotype. qPCR was performed to determine the expression of 4 different CSC markers (nestin-an intermediate filament-like protein, Musashi- a mRNA-binding protein that promotes Notch signaling by binding to the mRNA of Numb, the negative regulator of Notch signaling, thus preventing its translation, SOX2-a stem cell transcription factor and CD133-a cell surface transmembrane that is thought to organize cell membrane topology). While all markers appeared to be expressed in a cyclical fashion, nestin was the most reliably expressed marker throughout the course of the 10 passages. Therefore, it was determined that nestin expression could be used to predict the tumorogenesis of CSC cultures (Figure 2).

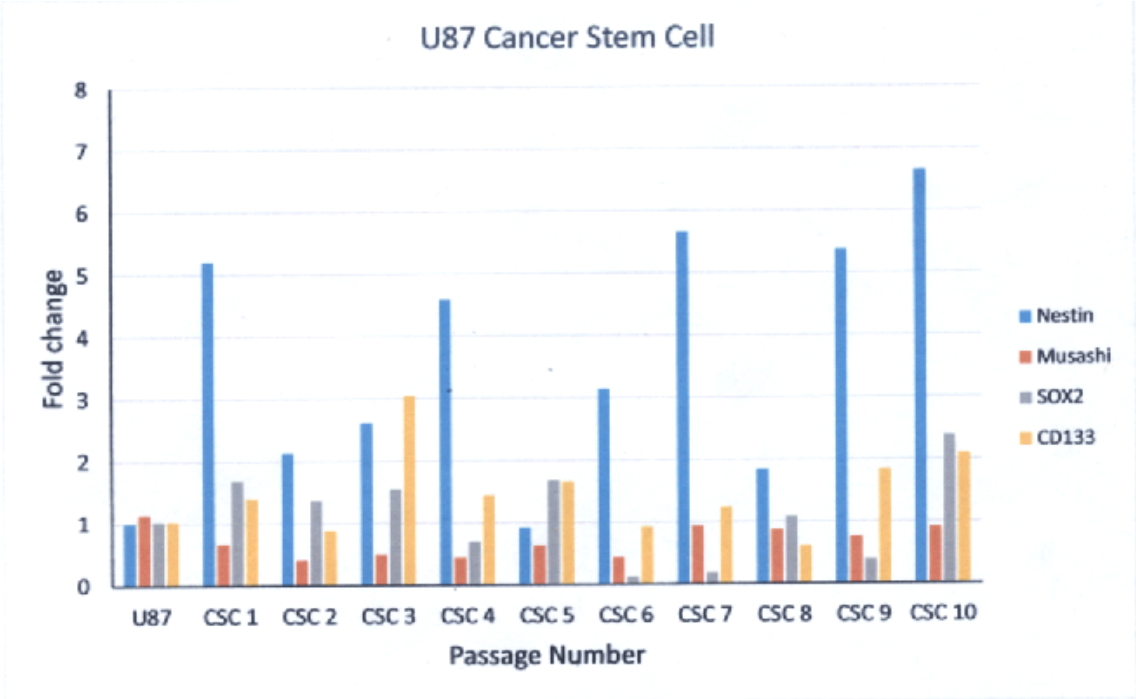

Figure 2. The presence of molecular markers for the CSC phenotype are another indicator of a CSC phenotype. The average relative changes in mRNA for the stem cell markers are plotted for up to 10 passages of the stem cell cultures (CSC1 through CSC10). Primers are shown in the table below. The level of nestin was used to predict the tumorigenesis of the CSC cultures. GADPH was used as the reference housekeeping gene.

With the formation of tumor-initiating spheres came the opportunity to perform a tumorigenesis experiment to look for further characteristics of stem cells. In the first experiment, 4×10^6 bulk cells were injected into one flank, resulting in the formation of tumors in all 4 subjects. The CSCs were injected in a lower concentration, 4×10^4. The CSCs did not initiate tumor growth in any of the four subjects. This unfortunate result was likely the product of low nestin expression in the injected population. The second experiment was more successful, with the majority of mice forming tumors after a concentration of 10^6 CSCs were injected. Similarly, tumors grew in all five mice when 2×10^6 CSCs were injected (Table 1). Ideally, a smaller concentration of CSCs would be injected than bulk cells. However,

the doubled rate of tumor growth was indicative of the presence of stem cells within the tumor-initiating spheres (Figure 3).

	# mice	# BULK CELLS INJECTED	BULK TUMOR GROWTH	# CSCs INJECTED	CSC TUMOR GROWTH
Expt. 1	4	4 x 10^6	4/4	4 X 10^4	0/4
Expt. 2	5	10^6	5/5	10^6	4/5
Expt. 3	5	2 X 10^6	5/5	2 X 10^6	5/5

Table 1. U87 CSC tumorigenesis experiment design

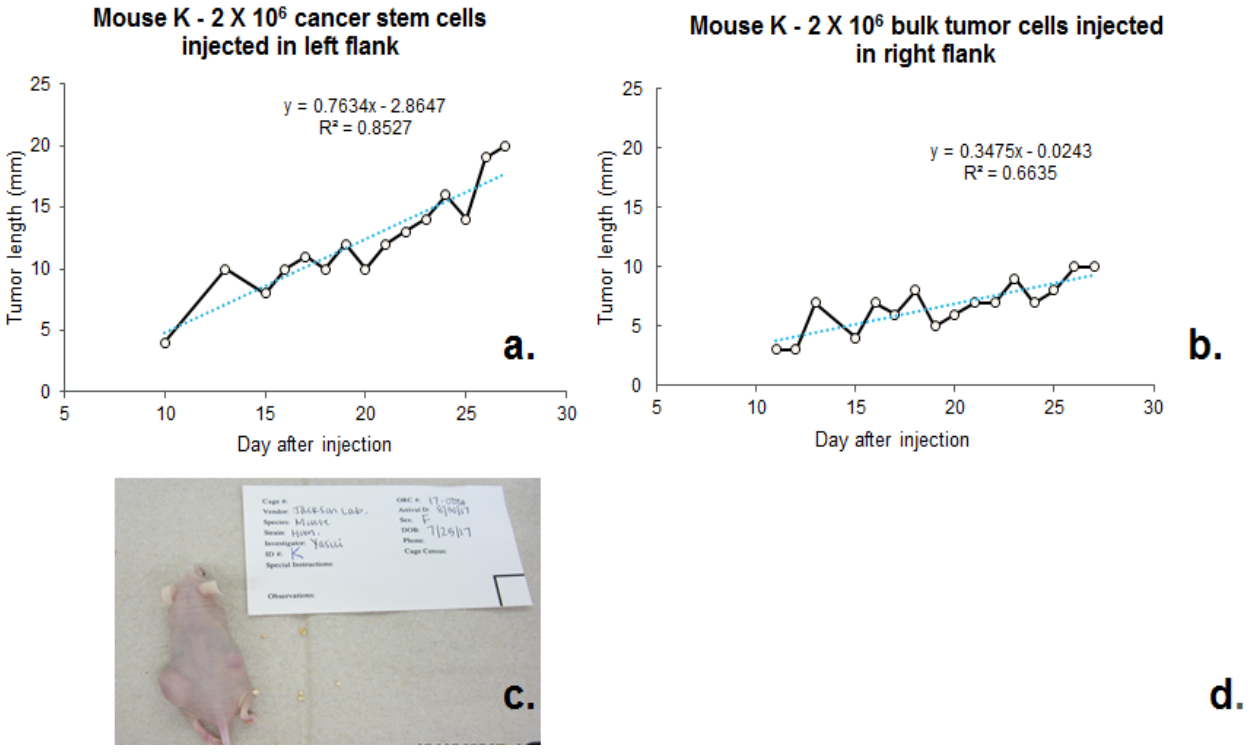

Figure 3. Tumorigenesis of U87 CSCs by xenotransplantation into BALBc athymic mice. In experiment 3, successful tumorigenesis was achieved when cells having high expression of nestin were injected into the flank of the mouse. Results show increased growth of CSCs (a) compared to bulk tumor cells (b). A representative mouse is shown in panel c having a CSC tumor in its left flank and a bulk cell tumor in its right flank. The overall health of the mouse remained stable as indicated by the stable weight of the mouse over the course of the 6-week experiment (d).

After completing the tumorigenesis experiment, the tumors were excised, embedded in paraffin and H & E stained. The images of the tumor sections showed key pathological features of a GBM tumor. Numerous mitotic structures were visible within the core of the tumor, indicating a high rate of proliferation. Additionally, the normal tissue surrounding the proliferating core was bordered by large areas of necrosis (Figure 4).

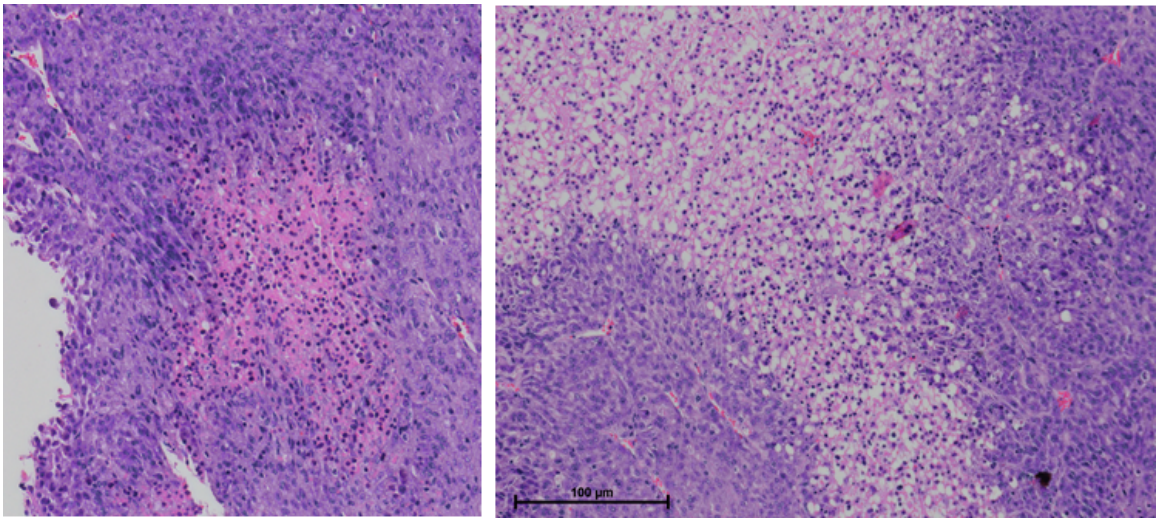

Figure 4. H & E stained paraffin embedded tumor sections illustrate the pathological features of GBM. The tumor section shown in panel a, shows numerous mitotic figures (dark purple stain in pink stained cells, indicating a high rate of proliferation in the tumor. Surrounding the tumor cells is the normal surrounding tissue (darker purple staining). Large areas of necrosis (lightest pink staining -> no stain) were observed as shown in panel b. The presence of necrosis is a key pathological character identifying GBM tumor.

Since all of the aforementioned experiments indicated a successful attempt at growing CSCs in culture, the culturing techniques could be applied to the DNA-PKcs KO cells to investigate their ability to form spheres. The DNA-PKcs KO cells also lost

contact inhibition in the NSCM; therefore, demonstrating similar sphere-formation processes first seen in the WT cells. However, when the cells were pelleted for TEM, it became evident that there were far fewer cells within the KO spheres when compared to WT spheres after 7 days (Figure 5). To determine whether this reduced cell count was a result of slow proliferation, a lack of proliferation, or lysing during preparation for TEM, a cell growth experiment was performed. A hemocytometer counting indicated that, while the U87 KO cells can form spheres, they are unable to proliferate as spheres. Unlike the WT spheres, which grew from less than 50,000 cells on day 0 to nearly 2,000,000 cells on day 6, the KO spheres maintained a cell count of less than 50,000 cells between day 0 and day 6 (Figure 6).

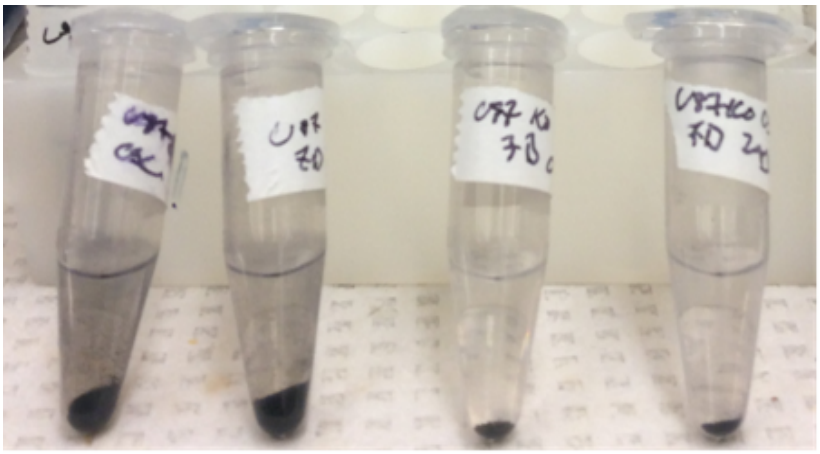

Figure 5. Next, we investigated what the U87 KO CSC sphere cells looked like by performing TEM. A small pellet size for the KO cells grown in NSCM as CSCs for 7 days compared to WT cells was observed in the TEM prep.

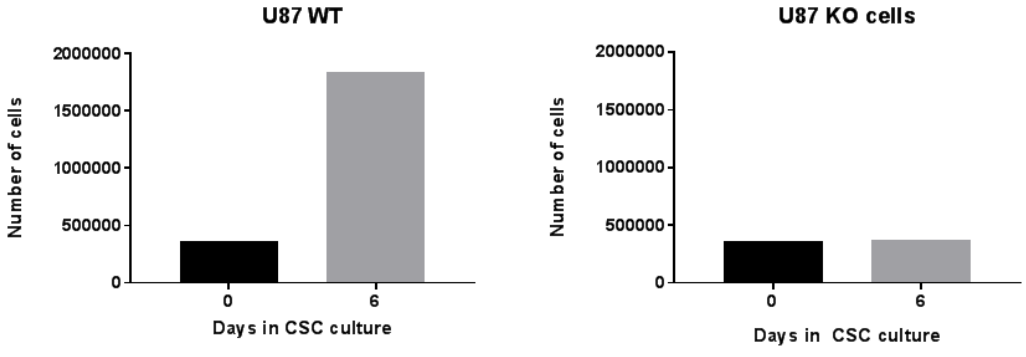

Figure 6. The U87 KO cells did not proliferate (but they did survive) in the NSCM sphere culture. A cell growth experiment to determine whether the KO cells had a slow rate of proliferation or did not proliferate or if the KO cells were simply more fragile and lysed during processing for TEM. Cell proliferation was measured by hemocytometer counting of whole U87 WT or U87 KO cells seeded into NSCM for CSC sphere culture on day 0 and compared to the number of single cells after 6 days in NSCM culture. Spheres were dissociated into single cell suspension using accutase for the cell quantification on day 6. A pronounced increase in cell number was found for WT U87 cells. Although spheres formed, the cell number did not change from the initial number of cells seeded for the U87 KO cells.

Assaying autophagy via TEM revealed interesting differences amongst the various populations of U87 cells. It was determined that the average number of autophagosomes per cell was 0.90 in U87 WT, 1.80 in U87 WT CSC, 1.90 in U87 WT CSC 2Gy, 0.80 in U87 KO, 1.20 in U87 KO CSC, 1.20 in U87 KO 2Gy, and 6.50 for U87 KO CSC 2Gy. Significant differences were observed between the U87 WT and U87 KO CSC 2Gy, U87 KO and U87 KO CSC 2Gy, U87 KO 2Gy and U87 KO CSC 2Gy, as well as U87 KO CSC and U87 KO CSC 2Gy (Figure 7). All of these groupings have a common denominator, U87 KO CSC 2Gy. The only large difference in autophagosome number was found in the irradiated population of U87 KO CSCs; however, this may have resulted from one cell that contained 31 autophagosomes, which was abnormally high when compared to the rest of the assayed cells under the same treatment conditions. Therefore, this cell may be a special, individual case, making it not representative of the sample as a whole. If this were the case, then the aforementioned differences would become insignificant.

While there was little difference in the average number of autophagosomes, significant changes in autophagosome morphology were observed. U87 KO cells exposed to 2Gy radiation contained complex autophagosomes that did not present with the typical membranous “halo” (Figure 8). However, U87 KO CSCs exposed to

2Gy radiation contained autophagosomes surrounded by membranous "halos" (Figure 9, b). In addition to this reversion to normal autohphagosome morphology in U87 KO CSCs exposed to 2Gy, mitochondrial morphology was altered in this population as well. Mitochondria lost the typical appearance of cristae due to many bubble structures filling the organelles. Additionally, mitochondria were swollen and numerous under these treatment conditions (Figure 9, a).

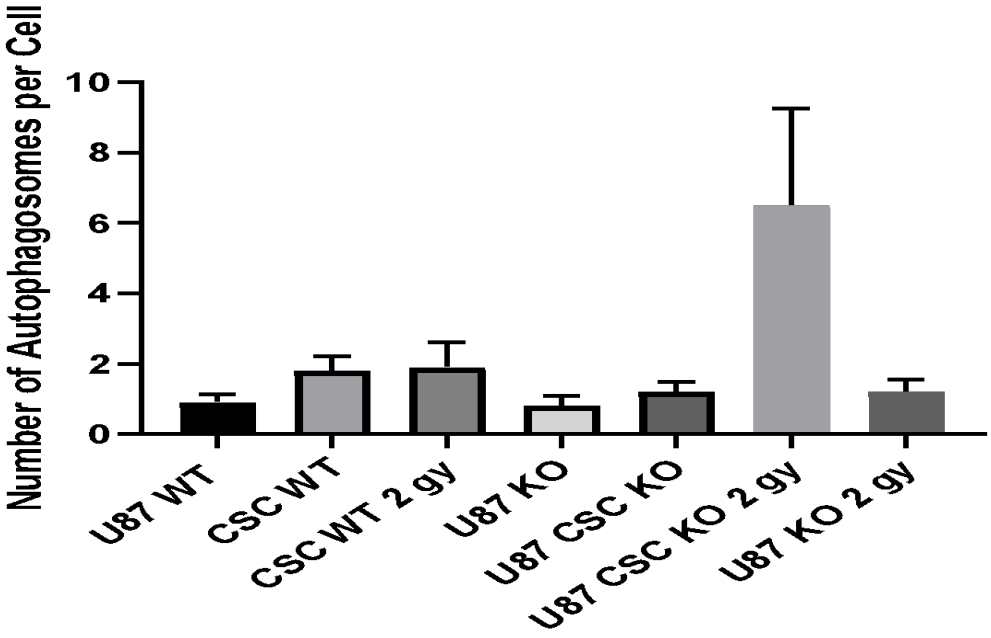

Figure 7. Preliminary morphometric analysis of autophagosomes per cell was performed. The number of autophagosomes were scored per cell using established criteria (Yasui et al., 2015; Bejarano et al., 2014) and plotted for the various cell lines and treatments. The mean values are plotted +/- SEM. The averaged data were analyzed by ANOVA and p values for statistical differences were calculated using a post-hoc Tukey test (GraphPad Prism 7.0).

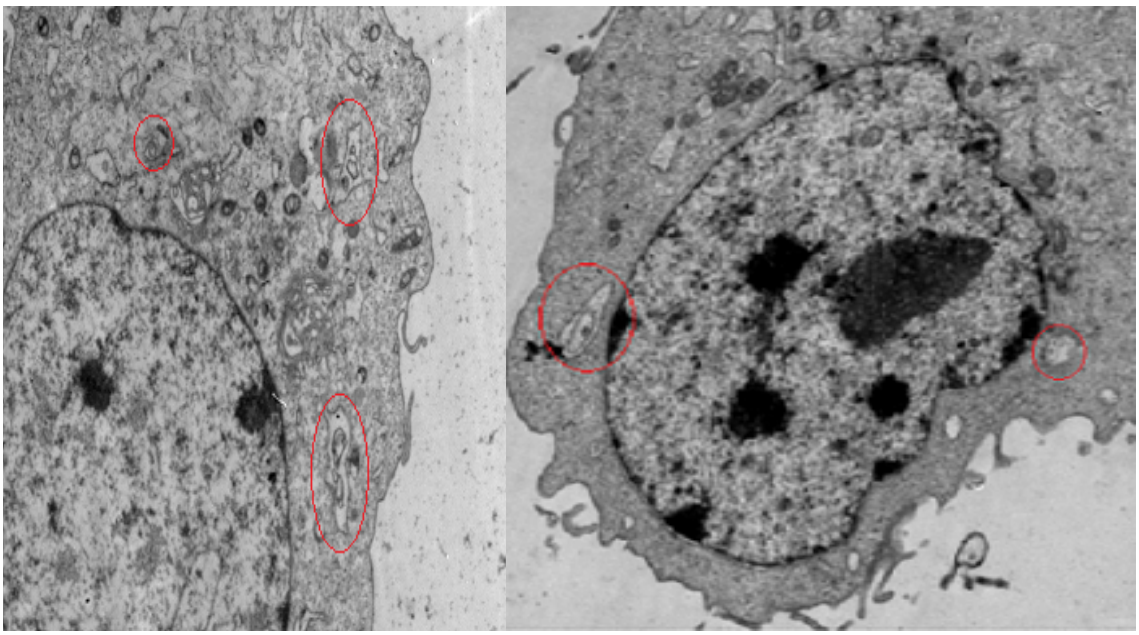

Fig. 8. TEM images of U87 KO cells exposed to 2 Gy. Autophagosomes are circled in red.

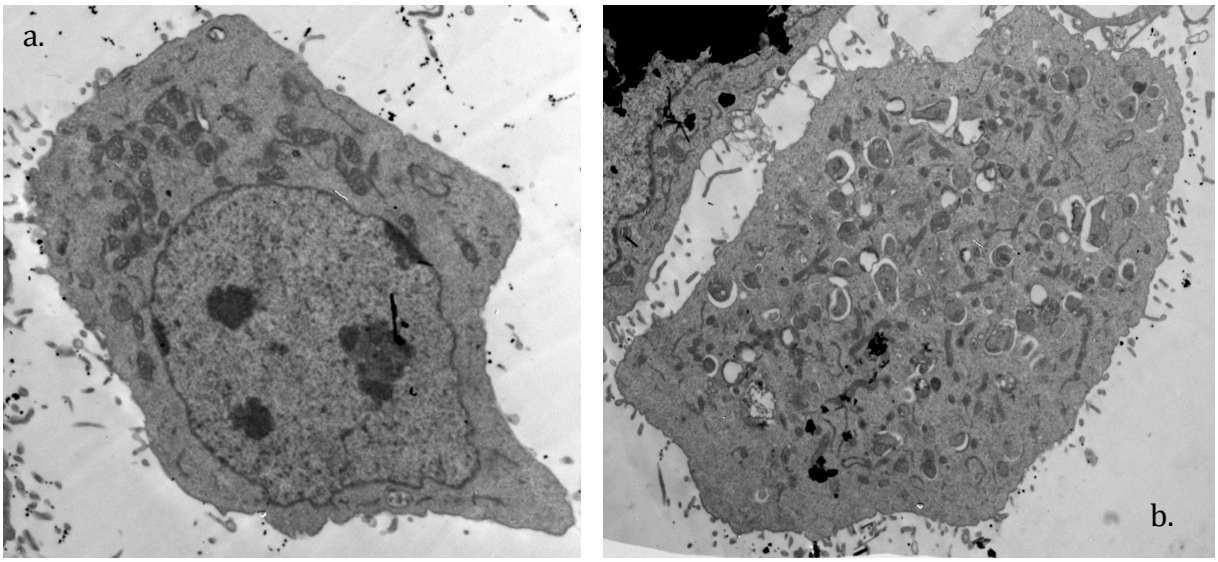

Figure 9. The U87 KO CSCs exposed to 2 Gy and cultured for 6 days after IR were metabolically compromised. Mitochondrial morphology (swollen and numerous) was changed (a) (12166) and numerous autophagosomes (structures that have "halos" around them) were found in some cells (12162) (b).

Preliminary ATP assay data revealed a 10-fold difference in ATP molecules amongst U87 WT and U87 KO cells. U87 WT cells contained 9×10^{12} ATP molecules per cell. U87 KO cells contained 8×10^{13} ATP molecules per cell.

Conclusion

While autophagy is often described as a housekeeping function, it is not unreasonable to believe that this stress response could lend clues regarding radiation sensitization, which is vital in the battle against GBM. Therefore, assaying the autophagy that resulted from a variety of treatments in U87 cell populations assists in understanding key cell stressors. DNA-PKcs, an enzyme that is important in the DNA damage response, was knocked out in an attempt to disrupt these processes and consequently stress cells. Additionally, stem cells were starved to encourage the stem cell phenotype and some groups of cells were irradiated- all increasing stress levels. The multitude of stressors was expected to increase levels of autophagy that precede cell death, but this was not the result.

The average number of autophagosomes remained relatively consistent across all cell treatments (Figure 7). Irradiated U87 KO CSCs averaged 6.5 autophagosomes per cell, which was significantly higher than the other averages. However, an outlier may have skewed this average; one cell in this population contained 31 autophagosomes, while the other individual cells in this group contained between 2 and 6 autophagosomes. Therefore, it is difficult to determine the significance of this difference in autophagy without assaying more irradiated knockout CSCs. Despite the questionable significance of the aforementioned

findings, noticeable differences in autophagosome morphology were observed in the U87 KO CSC 2Gy population when compared to the U87 KO 2Gy cells. The irradiated knockout cells contained complex autophagosomes that lacked the typical "halo" (Figure 8). CSCs under the same treatment conditions demonstrated an unexpected change in autophagosome morphology. The autophagosomes within the irradiated KO CSCs presented with more typical morphology and decreased complexity (Figure 9). This change is peculiar because the U87 KO CSC 2Gy condition is arguably the most stressful condition, yet the autophagy is more normal than that in the differentiated knockout cells exposed to radiation. It is difficult to determine what these changes in morphology indicate in the context of radiation sensitivity, so survival assays may provide information regarding the significance of these changes in morphology.

In addition to the morphological changes observed in CSC autophagosomes, irradiated knockout CSCs also presented with unusual mitochondria. The swollen, numerous mitochondria are indicative of a greater need for energy and stress placed specifically on these organelles. Preliminary ATP assay data only explored the number of ATP molecules per cell in WT and differentiated KO cells, but the changes in mitochondrial morphology will likely alter the number of ATP molecules per cell under extreme stress. No conclusions can be drawn from these values at this stage because there is no standard for comparison. Moving forward, more trials of this assay will be run and all cell treatments will be assayed. The visual assay of changes in mitochondria leads us to believe that directly assaying ATP levels will

reveal a change in the number of ATP molecules per cell when cells are exposed to more stressful conditions.

It must be mentioned that all of the previously stated data is preliminary. Therefore, we cannot draw definitive conclusions with the small amount of information we have collected. However, the data we have collected highlights the importance of noting morphological characteristics of autophagosomes and mitochondria in TEM images in addition to counting autophagosomes. The lab will continue to investigate the TEM images collected over the course of the spring semester, eventually assaying 30 images for each cell treatment to establish more reliable trends in autophagy. Additionally, the ATP assay will be run for all U87 cell populations/treatments to understand the impact of stressors on ATP metabolism. The interesting changes noted within the CSC populations are promising in the pursuit of a better understanding of these treatment resistant cells. Hopefully, understanding the importance of DNA-PK as not only a DNA damage repair molecule, but also an autophagy trigger will lead us to a better understanding of its overall importance in cancer cells. Any novel information can be used as ammunition in the war against cancer; therefore, while our findings are too preliminary to be suggestive, they do represent potential new avenues for exploration and inspire new, informed questions regarding the disease.

References

E Bejarano, A Yuste, B Patel, RF Stout, DC Spray, AM Cuervo. 2014. Connexins modulate autophagosome biogenesis. Nature Cell Biology 16, 401-414.

Davis, A. J., Chen, B. P., & Chen, D. J. (2014). DNA-PK: A dynamic enzyme in a versatile DSB repair pathway. *DNA Repair,17*, 21-29. doi:10.1016/j.dnarep.2014.02.020

Francesco, E. M., Sotgia, F., & Lisanti, M. P. (2018). Cancer stem cells (CSCs): Metabolic strategies for their identification and eradication. *Biochemical Journal,475*(9), 1611-1634. doi:10.1042/bcj20170164

Green DR, Galluzzi L, Kroemer G. 2014. Metabolic control of cell death. Science. 345(1250256):1–11.

Haines IE, Miklos GLG. 2014. Bevacizumab for newly diagnosed glioblast- oma. New Engl J Med. 370:2048–2049.

Levine B. 2007. Cell biology: autophagy and cancer. Nature. 446:745–747.

Livak KJ, Schmittgen TD. Analysis of Relative Gene Expression Data Using Real-Time Quantitative PCR and the 2-ΔΔCT Method. Elsevier Science. 2001; 25:402-408.

Marie SKN, Mieko S, Shinjo O. 2011. Metabolism and brain cancer. Clinics. 66:33–43.

Poteet E, Choudhury GR, Winters A, Li W, Ryou M-G, Liu R, Tang L, Ghorpade A, Wen Y, Yuan F, et al. 2013. Reversing the Warburg effect as a treatment for glioblastoma. J Biol Chem. 288:9153–9164.

Prophet, E. B., Mills, B., Arrington, J. B., & Sobin, L. H. (1992) *Armed Forces Institute of Pathology: Laboratory Methods in* Histotechnology Washington, D.C.: American Registry of Pathology

Sharma K, Goehe R, Beckta JM, Valerie K, Gerwitz DA. 2014. Autophagy and radiosensitization in cancer. SXCLI Jl. 13:178–191.

Stupp R, Hegi ME, Mason WP, van den Bent MJ, Taphoorn MJB, Janzer RC, Ludwin SK, Allgeier A, Fisher B, Belanger K, et al.; on behalf of the European Organisation for Research and Treatment of Cancer Brain Tumour and Radiation Oncology Groups and the National Cancer Institute of Canada Clinical Trials Group. 2009. Effects of radiotherapy with concomitant and adjuvant temozolomide versus radiotherapy alone on survival in glioblastoma in a randomised phase III study: 5-year analysis of the EORTC-NCIC trial. Lancet Oncol. 10:459–466.

Yang Z, Klionsky DJ. 2010. Mammalian autophagy: Core molecular machinery and signaling regulation. Curr Opin Cell Biol. 22:124–131.

Yasui LS, Johnson M, Savage H, Baker A, Baker E, Burns C. 2015. Measurement of radiation-induced autophagic flux in human brain cancer cells. Micros Microanal. 21:195–196.

Yasui LS, Owens K, 2012. Necrosis is not induced by gadolinium neutron capture in glioblastoma multiforme cells. International Journal of Radiation Biology 88, 980–990.

Zois CE, Koukourakis MI. 2009. Radiation-induced autophagy in normal and cancer cells. Autophagy. 5:442–450.